RESEARCH PAPER

Investigation of the Effect of Calcination Time on the Antibacterial, Antifungal and Anticancer Activities of TiO_2/ZnO Nanocomposites

Adil Kadum Shakir[1,*], Ebrahim Ghanbari-Adivi[1], Aref S. Baron[2,3], Morteza Soltani[1]

* *nnanoscale@gmail.com*

[1] Faculty of Physics, University of Isfahan, Isfahan 8174673441, Iran
[2] Department of Physics, College of Science, University of Kufa, Al-Najaf, Iraq
[3] Department of Sonar, College of Medical and Health Technologies, University of Alkafeel, Al-Najaf, Iraq

Received: October 2024 **Revised: February 2025** **Accepted: March 2025**
DOI: 10.22068/ijmse.3778

Abstract: *Nanomaterials have significantly transformed multiple scientific and technological fields due to their exceptional properties resulting from their quantum confinement effects and high surface-to-volume ratios. Among these materials, zinc oxide (ZnO) and titanium dioxide (TiO_2) nanoparticles have attracted considerable interest because of their diverse applications.*

In this study, TiO_2-ZnO nanocomposites were synthesized using varying calcination times of 1, 1.5, 2, 2.5, and 3 hours. Characterization of fabricated samples through X-ray diffraction (XRD) spectroscopy, Fourier transform infrared (FTIR) spectroscopy, field emission scanning electron microscopy (FESEM), and energy-dispersive X-ray spectroscopy (EDXS) confirmed the successful fabrication of the nanocomposites. In this regard, XRD analysis revealed anatase TiO_2 and hexagonal wurtzite ZnO phases. Raman spectroscopy also supported these findings, identifying characteristic peaks of both TiO_2 and ZnO.

The calcination time had a minimal effect on the crystal structures and the nanocomposites' morphology, which gave rise to its negligible impact on the samples' optical properties and biological activities. Optical properties assessed using UV-visible and photoluminescence (PL) spectroscopy showed consistent band gap absorption and emission profiles across all samples, among which the nanocomposite calcined for 1 hour exhibited the best optical properties. The sample prepared at 1 hour showed the most favorable optical properties and significant antibacterial, antifungal, and cytotoxic activities, making it suitable for various applications. In this regard, more than 99.9% reduction occurred in the number of Escherichia coli, Staphylococcus aureus bacteria, and Candida albicans fungus using TiO_2-ZnO nanocomposite. Besides, adding 500 µg/ml of nanocomposite decreased the cell viability to 34.47%, which signifies its high cytotoxicity activity.

Keywords: *TiO_2-ZnO nanocomposite, Calcination time, Zinc oxide, Titanium dioxide, Antibacterial activities.*

1. INTRODUCTION

Recent advances in nanotechnology have facilitated the investigation of particles whose sizes vary from 1 to 1000 nanometers. Compared to their larger counterparts, the small dimensions of these particles have resulted in their unique properties, making them appealing for numerous applications in various sectors, including electronics, renewable energy, environmental remediation, and biomedical research [1, 2]. Many studies have demonstrated that nanomaterials possess enhanced mechanical, electrical, magnetic, thermal, catalytic, and antimicrobial properties compared to larger-scale counterparts. Beyond their applications in nanomedicine, nanomaterials are also influential in other fields, such as nanoelectronics, biomaterials, energy production, and consumer products. Furthermore, nanotechnology holds the promise of developing a variety of novel materials and devices [3].

Thanks to their characteristics, for instance, their high ability in the decomposition of organic and inorganic pollutants originating from photocatalytic properties and also extraordinary antimicrobial and antifungal activities, Zinc oxide (ZnO) and titanium dioxide (TiO_2) have been employed in a range of applications, consisting of biomedical, fabrication of electrodes for water splitting, hydrogen generation, carbon dioxide reduction, solar energy conversion, drug delivery systems, sensors, and energy storage solutions. Some strategies, such as doping and the creation of nanocomposites, have been used to enhance the antifungal effectiveness of these nanoparticles [4-6]. These materials typically act as n-type semiconductor photocatalysts, breaking down various organic contaminants in air and wastewater. The band gap and excitation binding energies for ZnO and TiO_2 are relatively high, approximately 3.3 eV and 60 meV for ZnO and 3.1 eV and 53 meV for TiO_2, respectively. The

[DOI: 10.22068/ijmse.3778]

energy required for photon-induced electron excitation, allowing the transition of electrons from the valence band (VB) to the conduction band (CB), primarily occurs within the ultraviolet (UV) spectrum [4].

Among many semiconductor nanomaterials, TiO_2 and ZnO have gained significant attention because of their excellent chemical stability, low toxicity, affordability, and strong antimicrobial properties [6]. The antibacterial and antifungal characteristics of metal oxide nanoparticles have been extensively investigated. The findings obtained from the research indicate that ZnO demonstrates antibacterial effects and can boost the generation of reactive oxygen species (ROS) as its particle size decreases. Its antifungal properties arise from the generation of free radicals on the nanoparticles' surfaces, which damage the lipids in fungal cell membranes, subsequently resulting in protein leakage through disrupted membranes [5, 6].

TiO_2 nanoparticles exhibit antimicrobial effects even at minimal concentrations through a photocatalytic mechanism that inflicts severe damage to the targeted microorganisms. Both anatase and rutile phases of TiO_2 nanoparticles are known for their excellent antifungal properties. The widespread usage of titanium dioxide is attributed to its exceptional thermal and chemical stability and high photocatalytic performance. The toxicity associated with titanium dioxide nanoparticles stems from their physical characteristics rather than their chemical composition. These nanoparticles can cross biological barriers, potentially causing harm to cells or organs. Various methods have been employed to enhance the antimicrobial efficacy of titanium dioxide nanoparticles against simple microorganisms such as bacteria and viruses [5].

To overcome the challenges posed by wide band gaps and low photoenergy conversion efficiency, researchers have investigated the hybridization of noble metals with semiconducting oxides like ZnO and TiO_2. This strategy seeks to enhance the photocatalytic activity of the nanoparticles by integrating their energy levels at the heterojunction [7, 8]. Therefore, in recent years, the development of hybrid nanomaterials has attracted considerable attention within the nanotechnology sector. These innovative materials can modify individual particles' properties while introducing new and improved functionalities. However, specific nanostructures, such as ZnO, are often characterized by limited optical properties and have point defects, which can restrict their direct application in different industries [9, 10]. An up-and-coming area of research is the creation of nanohybrid ZnO/TiO_2 materials, which merge the beneficial properties of both components. These nanohybrids have demonstrated significant potential in applications related to antibacterial, antifungal, and anticancer activities, particularly in the context of treating skin cancer [11, 12].

Recent research has shown that the synergetic effects of ZnO and TiO_2 nanoparticles can lead to improved antimicrobial effectiveness against multidrug-resistant bacteria and better biocompatibility [13-15]. Therefore, as mentioned above, combining ZnO and TiO_2 is one of the most straightforward methods to enhance these metal oxides' antibacterial and antifungal properties. Although numerous studies have investigated the antibacterial and antifungal effects of each ZnO and TiO_2, the specific antibacterial and antifungal performance of TiO_2-ZnO hybrid nanomaterials has not been thoroughly explored in the literature [16]. In a study, Najibi Ilkhechi et al. [5] synthesized ZnO, TiO_2, and ZnO–TiO_2 composite (1:1 weight ratio) using the sol-gel method. All the prepared nanoparticles inhibited the fungi growth at the concentration of 50 μg/ml, among which the TiO_2-ZnO composite exhibited superior antifungal activities compared to TiO_2 and ZnO. At 300 μg/ml, TiO_2 and TiO_2-ZnO composite completely inhibited spur production. The morphology of the particles varied where pure ZnO was pyramidal, TiO_2 showed a spherical-shaped structure, and the TiO_2-ZnO composite exhibited a combination of both shapes, as mentioned above, along with additional surface growth. Notably, TiO_2-ZnO composite at lower concentrations (150 μg/ml) can increase ROS production and produce more oxidative stress than pure TiO_2 or ZnO, enhancing its antifungal activities.

In another research, Gunasekaran et al. [3] synthesized pure ZnO and ZnO-doped TiO_2 nanocomposites via a sol-gel method to degrade methylene blue (MB) under visible light. ZnO-doped TiO_2 composite achieved an 84% degradation rate over 6 hours. Kinetic analysis showed that the degradation process follows pseudo-first-order kinetics. Additionally, the

[DOI: 10.22068/ijmse.3778]

ZnO-doped TiO_2 nanocomposites exhibited enhanced antibacterial activities, which could effectively inhibit both Gram-positive and Gram-negative bacteria, including Escherichia coli and Bacillus sublittus. Also, Siwinska-Stefańska et al. [17] delineated the creation of a multifunctional TiO_2–ZnO composite through a hydrothermal approach, which exhibited strong photocatalytic capabilities. The influence of two critical parameters, including reaction time and the molar ratio of TiO_2 to ZnO, was investigated in this study on the physicochemical and structural attributes of the binary system during hydrothermal synthesis. Their findings indicated that improvement in various properties, consisting of morphology, crystallinity, porosity, and chemical surface characteristics, can enhance photocatalytic and antibacterial activities.

This study aims to focus on the synthesis of nanohybrid ZnO/TiO_2 materials and assess their optical properties and antibacterial and antifungal activities.

2. EXPERIMENTAL PROCEDURES

To fabricate ZnO nanoparticles, 8.76 gr of zinc acetate ($Zn(CH_3CO_2)_2$) and 3.19 gr of sodium hydroxide (NaOH) were separately dissolved in 20 mL of water, followed by incessant stirring at 35°C for 20 minutes. Next, the prepared solutions were mixed and stirred for 2 hours until the formation of a milky solution. Afterwards, the resulting solution was subjected to another 100-minute stirring until the conversion of the solution into a gel-like substance.

In a separate stage, to synthesize TiO_2, 15 mL of titanium tetraisopropoxide (TTIP) was dissolved in 50 mL of ethanol and continuously stirred for 30 minutes. Then, 20 mL of deionized water was added to the resulting solution and stirred until the formation of a white solution.

Finally, for the fabrication of nanohybrid TiO_2-ZnO, the white solution obtained in the previous stage was mixed with the gel-like substance prepared in the first step and left at room temperature for 240 minutes. Afterwards, the resulting mixture was centrifuged eight times (each centrifuge took 10 minutes and was performed at 10,000 rpm). Then, the product was dried in an oven at 150°C for 10 hours. The dried product was placed in a furnace and calcinated at 700°C for five durations of 1, 1.5, 2, 2.5, and 3 hours.

3. RESULTS AND DISCUSSION

The X-ray diffraction (XRD) images of the TiO_2-ZnO nanocomposites calcinated at 700°C, and various times of 1, 1.5, 2, 2.5, and 3 hours are illustrated in Figure 1. XRD is an advantageous and powerful means of studying materials from a crystallographic aspect. All the XRD images were collected in the 2θ ranging from 5 to 75 degrees. According to the XRD image of the nanocomposite composed of ZnO and TiO_2 and calcinated at one h (Figure 1a), the peaks located at approximately 25.3, 36, 49, 53.5, 54.3, 63.4, 68.9, and 70.9 degrees can be ascribed separately to the (101), (004), (200), (105), (211), (204), (116), and (220) planes of anatase TiO_2. In addition, other peaks, including 32.8, 35.4, and 56.7 degrees, respectively, related to the (100), (101), and (110) planes of the hexagonal wurtzite ZnO phase, can be seen [18-22]. The XRD peaks detected for the TiO_2 and ZnO verify the successful synthesis of the nanocomposite.

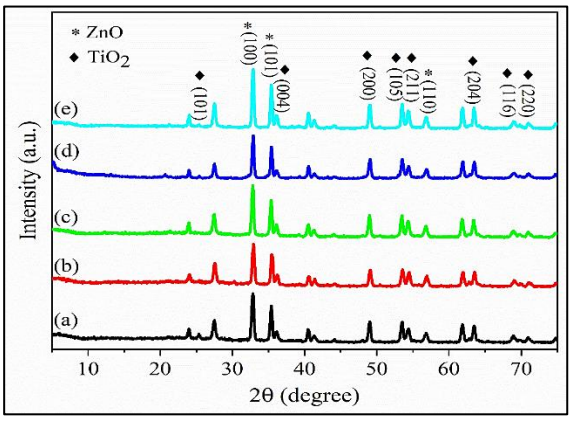

Fig. 1. The XRD images of the TiO_2-ZnO nanocomposites calcinated at (a) 1, (b) 1.5, (c) 2, (d) 2.5, and (e) 3 hour (s)

As evidenced by the XRD image of the nanocomposite obtained at 1.5 h, the increment in the calcination time had a negligible impact on the crystal structure of the nanocomposite (Figure 1b). Based on this fact, the peaks related to the TiO_2 and ZnO observed for the sample obtained at 1 h are also detected for the one calcinated at 1.5 h. Raising the calcination time from 1.5 to 2 h has attenuated the intensity of the (101) peak at 25.3 degrees (Figure 1c). However, the major peaks related to TiO_2 and zinc oxide can

[DOI: 10.22068/ijmse.3778]

be easily observed.
Like the nanocomposites calcinated at 1 and 1.5 h, the one obtained at 2.5 h shows the main peaks of TiO_2 and ZnO (Figure 1d). Accordingly, the planes related to the TiO_2 and zinc oxide found in the XRD pattern of the nanocomposite calcinated at 1 h can be easily detected for the sample calcinated at 2.5 h. Increasing the calcination time from 2.5 to 3 h also had no considerable impact on the structure of the nanocomposite. According to the XRD image of the nanocomposite synthesized at 3 h (Figure 1e), the increment in the calcination time did not change the positions of the XRD peaks and their intensities. Besides, the planes relevant to the TiO_2 and the ZnO can be detected. In conclusion, the calcination time insignificantly altered the structure of the nanocomposites, and all the prepared samples disclosed similar XRD patterns.
Fourier transform infrared spectroscopy (FTIR) was adopted to scrutinise the functional groups, such as vibrational inorganic metallic modes present within the TiO_2-ZnO nanocomposites. Figure 2 exhibits the FTIR spectra of the nanocomposites fabricated at varied calcination times. Referring to the FTIR spectrum of the nanocomposite obtained at a calcination time of 1 h (Figure 2a), the peak found at the wavenumber of 3430 cm^{-1} is typically ascribed to the absorption band of hydroxyl (O–H) of H_2O molecules within the nanocomposite.

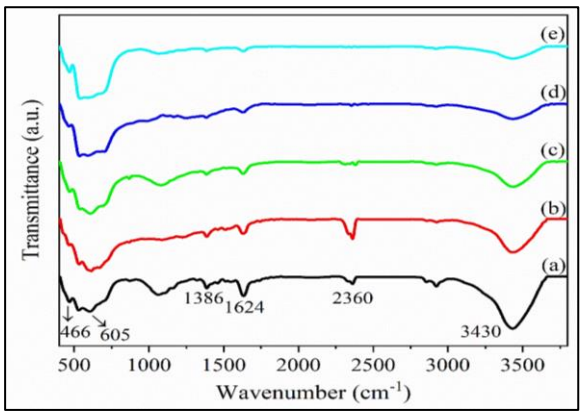

Fig. 2. The FTIR spectra of the TiO_2-ZnO nanocomposites synthesized at the times of (a) 1, (b) 1.5, (c) 2, (d) 2.5, and (e) 3 hour (s)

The absorption band detected at approximately 2360 cm^{-1} corresponds to the C-O bending of physisorbed carbon dioxide (CO_2) molecules in the air [23]. The peaks observed at the 1624 and 1386 cm-1 wavenumbers can be attributed to the remaining sp^2 carbon and tertiary C–OH groups. According to references, the stretching modes of inorganic metallic bonds are usually detected in the range from 400 to 800 cm^{-1} [24]. As a result, the broad characteristic peak situated at about 605 cm^{-1} is pertinent to the stretching vibrations of Ti–O bonds [25]. Moreover, the pronounced peak seen at the wavenumber of 466 cm^{-1} is relevant to the Zn-O bond [26-28]. The peaks found in the FTIR spectrum of the TiO_2-ZnO nanocomposite calcinated at 1 h corroborate the successful synthesis of the nanocomposite.
Raising the calcination time from 1 to 1.5 h does not affect the FTIR spectrum of the TiO_2-ZnO nanocomposite (Figure 2b). Accordingly, the absorption band of the O-H bond in H_2O molecules, the peak corresponding to the physisorbed CO_2 molecules, and the absorption bands assigned to the residual sp^2 carbon and tertiary C–OH groups can easily be detected. Moreover, the characteristic peaks pertinent to the Ti–O and Zn-O bonds can be observed.
Figure 2c illustrates the FTIR spectrum of the TiO_2-ZnO nanocomposite prepared at the time of 2 h, which is taken in the range approximately from 500 to 3750 cm^{-1}. Obviously, the peak pertinent to the O-H bond in H_2O molecules is observed. Moreover, the peak demonstrating physisorbed CO_2 molecules, the peak showing the residual sp^2 carbon, and the peak related to the tertiary C–OH groups can be seen. Ti–O and Zn-O bond peaks are detectable for the TiO_2-ZnO nanocomposite calcinated at 2 h, implying the successful fabrication of the sample.
The increment in the calcination times of the TiO_2-ZnO nanocomposites from 2 to 2.5 h and also from 2.5 to 3 h has inconsiderably influenced the FTIR spectra of the samples (Figures 2d, e). Analogous to other TiO_2-ZnO nanocomposites, the well-defined peaks of Ti–O bonds found at 605 cm^{-1} and the peak of Zn-O observed at 466 cm^{-1} can also be seen for the nanocomposites synthesised at the times of 2.5 and 3 h. As the FTIR spectra of the nanocomposites disclosed, increasing the calcination time had a negligible effect on their spectra. Also, similar FTIR spectra were shown in all the samples.
Field emission scanning electron microscopy (FE-SEM) was chosen to morphologically investigate the prepared TiO_2-ZnO nanocomposites, and the FESEM images recorded from the surface

[DOI: 10.22068/ijmse.3778]

of the samples are demonstrated in Figure 3. As evidenced by the FESEM image of the TiO_2-ZnO nanocomposite calcinated at the time of 1 h (Figure 3a), the spherical-shaped titanium dioxide particles and the rod-type zinc oxide nanoparticles are visible [18]. The size of the round-shaped TiO_2 particles exceeds 1 µm. However, the ZnO particles possess a nanometer scale. By raising the calcination time to 1.5 h, no noticeable change is observed in the morphology of the TiO_2-ZnO nanocomposite (Figure 3b). Accordingly, the rod-shaped ZnO nanoparticles are also detected for the TiO_2-ZnO nanocomposite prepared at 1.5 h. The round-shaped TiO_2 particles are buried under the rod-shaped ZnO nanoparticles. No change was detected in the size of the titanium dioxide and zinc oxide particles while the calcination time increased. Like other samples, in the FESEM image of the TiO_2-ZnO nanocomposite prepared at the time of 2 h, the TiO_2 particles having a round shape and the ZnO nanoparticles having a rod shape are discovered (Figure 3c). With increasing the calcination time, no visible change can be found in the diameter of titanium dioxide and zinc oxide particles.

The rise in the time of the calcination process from 2 to 2.5 h has resulted in the appearance of some agglomerated particles. Based on Figure 3d, the ZnO particles having the shape of a rod are detected for the TiO_2-ZnO nanocomposite obtained at the time of 2.5 h; however, some agglomerated ZnO particles can be found in this sample, which was not observed in the TiO_2-ZnO nanocomposites calcinated at the times of 1, 1.5, and 2 hours. Analogous to the sample synthesized at the time of 2.5 h, the one fabricated at the time of 3 h manifests the agglomerated ZnO particles (Figure 3e), meaning that increasing the calcination time to the 2.5 and 3 h can cause the production of agglomerated ZnO particles, which can negatively affect the optical and also antibacterial performance of the TiO_2-ZnO nanocomposite.

Figure 4 demonstrates the energy dispersive X-ray spectroscopy (EDXS) patterns of the nanocomposites synthesized at varied times, consisting of 1, 1.5, 2, 2.5, and 3 hours. The EDXS is a beneficial technique to investigate the chemical composition of the materials.

Based on the EDXS pattern of the nanocomposite calcinated at the time of 1 h (Figure 4a), the characteristic peaks of Ti element found at approximately 0.5, 4.5, and 5 keV testify the presence of the titanium-containing species within the nanocomposite. In addition to the Ti element, some Zn peaks relevant to the zinc-based particles are detected, which are situated at 1, 8.5, and 9.5 keV.

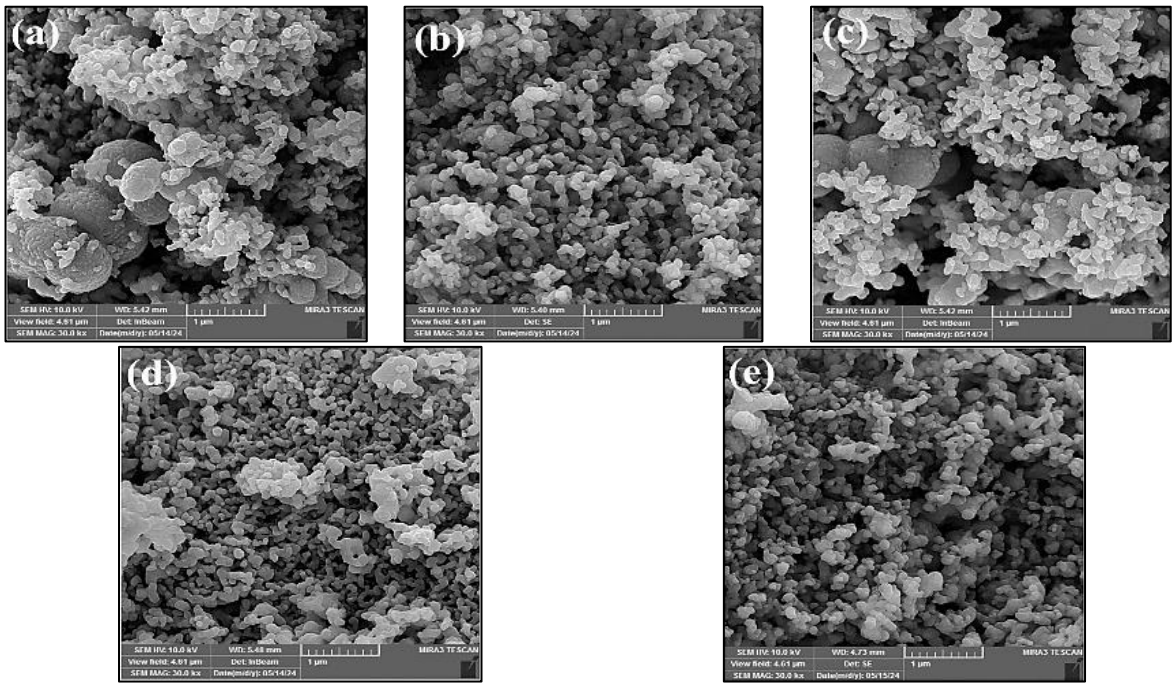

Fig. 3. The FESEM images taken from the TiO_2-ZnO nanocomposites calcinated at the times of (a) 1, (b) 1.5, (c) 2, (d) 2.5, and (e) 3 hour (s)

[DOI: 10.22068/ijmse.3778]

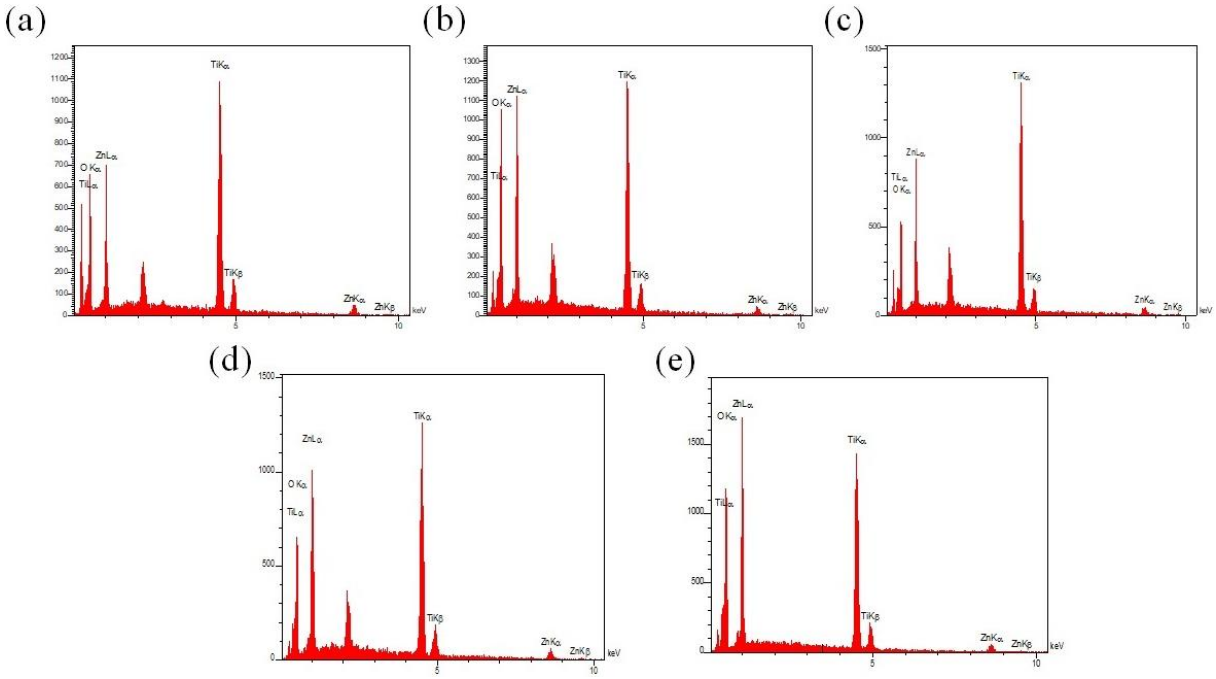

Fig. 4. The EDXS pattern of the TiO_2-ZnO nanocomposites prepared at the times of (a) 1, (b) 1.5, (c) 2, (d) 2.5, and (e) 3 hour (s)

The peaks showing the existence of the titanium- and zinc-containing species inside the nanocomposite are also observed in the EDXS pattern of the sample constructed at 1.5 hours. In this regard, the pronounced peaks of Ti and Zn elements are easily seen (Figure 4b).

Raising the calcination time from 1.5 to 2, 2.5, and 3 hours had no influence on the chemical composition of the nanocomposite (Figures 4c, d, e). The EDXS patterns of the nanocomposites calcinated at 2, 2.5, and 3 hours exhibit the major peaks of Ti and Zn elements, which attest to the presence of titanium- and zinc-containing species.

In the Raman spectrum of the nanocomposite calcinated at the time of 1 h (Figure 5a), the peaks located at about 140.7 and 609.8 cm^{-1} can separately be imputed to the vibrations of E_g and B_2g of anatase TiO_2 [19, 20]. The peak at ~341.9 cm^{-1} is associated with the multiple phonons scattering of zinc oxide. In addition to this peak, another peak verifying the presence of the zinc oxide nanoparticles appears at 446.6 cm^{-1}, which stems from the E_2 vibrational mode of the oxygen (O) atoms inside the zinc oxide particles. At 710.7 cm^{-1}, a peak is found because of the E_1 mode of zinc oxide [19, 20]. Raising the calcination time to 1.5 h has resulted in a significant change in the Ranam spectroscopy of the nanocomposite (Figure 5b). According to the Raman spectrum of the nanocomposite obtained at the time of 1.5 h, the peaks relevant to the anatase TiO_2 and wurtzite ZnO seen in Figure 5a have completely disappeared.

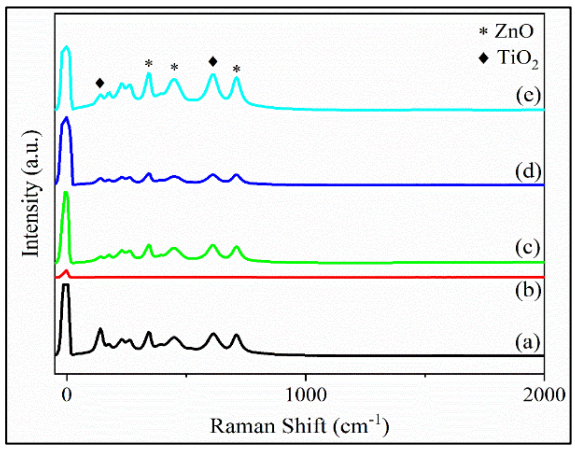

Fig. 5. The Raman spectra of the nanocomposites calcinated at the times of (a) 1, (b) 1.5, (c) 2, (d) 2.5, and (e) 3 hour (s)

However, the change in the calcination time from 1.5 to 2 h led to the appearance of the Raman peaks not found for the nanocomposite calcinated at 1.5 h (Figure 5c). Accordingly, the Raman peaks at 140.7 and 609.8 cm^{-1} relevant to the vibrations of E_g and B_2g of anatase titanium dioxide are visible. Besides, the peak at 341.9

[DOI: 10.22068/ijmse.3778]

cm^{-1} is assigned to the multiple phonons scattering of zinc oxide, the peak at 446.6 cm^{-1} is assigned to the E_2 mode of the O atoms within the zinc oxide particles, and the peak at 710.7 cm^{-1} owing to the E_1 mode of zinc oxide can easily be detected. Like other samples, the TiO_2-ZnO nanocomposites calcinated at the times of 2.5 and 3 h reveal the peaks related to the titanium dioxide and zinc oxide (Figure 5d, e). As the characterization tests of XRD, FTIR, FESEM, EDXS, and Raman corroborated, the TiO_2-ZnO nanocomposites were successfully fabricated at different times of 1, 1.5, 2, 2.5, and 3 hours.

The optical properties of the nanocomposites calcinated at 1, 1.5, 2, 2.5, and 3 h were measured using UV-visible spectroscopy. Figure 6a demonstrates the diffuse UV-visible spectrum of the TiO_2-ZnO nanocomposite prepared at the calcination time of 1 hour. Accordingly, a strong and broad absorption peak is clearly observed in the 300 to 400 nm wavelength. This peak is located in the UV region and shows the band gap absorption edge [21]. The increment in the calcination time has resulted in no noticeable change in the UV-visible spectrum of the TiO_2-ZnO nanocomposites, and no redshift or blueshift occurred. Referring to the diffuse UV-visible spectrum of the TiO_2-ZnO nanocomposite obtained at the time of 2 h (Figure 6b), the strong and broad peak seen in Figure 6a is also found for this sample. As a result, the nanocomposite possesses an optical property in the UV region, arising from inter band electronic transitions.

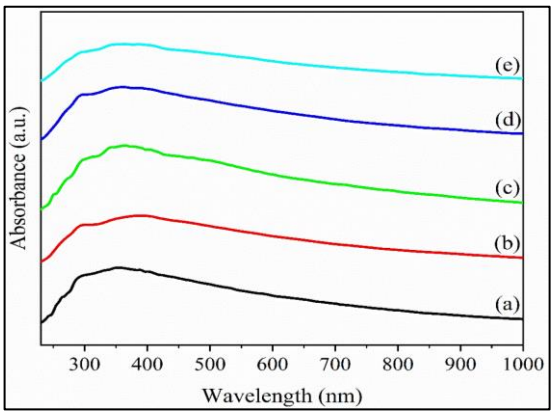

Fig. 6. The UV-visible spectra of the TiO_2-ZnO nanocomposites calcinated at the times of (a) 1, (b) 1.5, (c) 2, (d) 2.5, and (e) 3 hour (s)

Like the nanocomposites calcinated at 1 and 1.5 h, the one prepared at 2 h exhibits a strong and broad absorption peak in the wavelength ranging from 300 to 400 nm (Figure 6c). No change can be detected in the absorption peak's position with the increasing calcination time. In other words, no redshift or blueshift is observed with the increment in the calcination time. The peak in the range from 300 to 400 nm is situated in the UV region, which originates from the inner band electronic transitions.

The broad peak in the UV region can be found in the spectrum of the nanocomposite fabricated at 2.5 hours (Figure 6d). Like other samples, this peak is located in the range from 300 to 400 nm, which is evidence for possessing the nanocomposite from an optical property in the UV region. Figure 6e exhibits the diffuse UV-visible spectrum of the TiO_2-ZnO nanocomposite calcinated at the time of 3 h. As we saw for the aforementioned samples, this nanocomposite also manifests the absorption peak in the UV region, which ranges from 300 to 400 nm in the wavenumber. Consequently, all the TiO_2-ZnO nanocomposites calcinated at different times take advantage of an optical property in the UV region. In addition, with increasing the calcination time, no noticeable change was observed in the position of the absorption peak.

Figure 7 illustrates the photoluminescence (PL) images of the nanocomposites calcinated at the times of 1, 1.5, 2, 2.5, and 3 h. Two emission peaks can commonly be found in metal oxide materials, one of which is observed in the UV region and is related to near band edge emissions. The other peak is usually detected in the visible region, which arises from the deep-level emissions. The former has strong intensity and stems from the free exciton recombination. But, the latter possesses weaker intensity and arises from oxygen defects. Deep-level emissions are seen in the visible region and are made from recombining photogenerated holes. The visible spectrum typically comprises several individual parts, including UV-violet, violet, violet-blue, blue, and green sections located roughly at 395, 423, 458, 500 and 501 nm [22-28].

Figure 7a demonstrates the PL image of the nanocomposite synthesized for 1 hour. Accordingly, a sharp peak is found near the wavelength of 350 nm in the UV region. In addition to this peak, another peak can be detected at the wavelength near 700 nm, which is weaker than the one seen at 350 nm. The peak at 700 nm is in the red section

[DOI: 10.22068/ijmse.3778]

of the visible region and is imputed to the deep-level emission. The increasing the calcination time of the TiO_2-ZnO nanocomposites from 1 to 1.5 h has led to no obvious change in the position of the PL peaks. As evidenced by PL spectrum of the nanocomposite obtained at 1.5 hours (Figure 7b), the sharp peak at 350 nm in the UV region and the peak at 700 nm in the visible region are found.

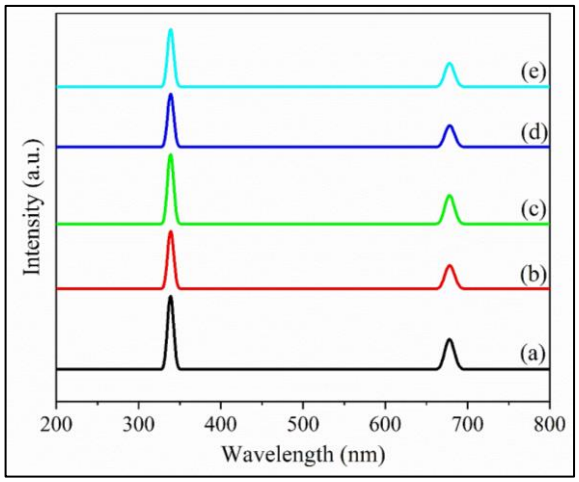

Fig. 7. The PL spectra of the TiO_2-ZnO nanocomposites were prepared at (a) 1, (b) 1.5, (c) 2, (d) 2.5, and (e) 3 hour (s)

Analogous to nanocomposites prepared at 1 and 1.5 h, the one calcinated at 2 h shows the PL peaks at 350 and 700 nm. Accordingly, in the PL image of the nanocomposite obtained at 2 h (Figure 7c), two well-defined peaks at 350 and 700 nm are detected, respectively, in the UV and visible regions. Figure 7d and showing the PL images of the nanocomposites calcinated at 2.5 and 3 hours, respectively; two pronounced peaks are visible, located at 350 and 700 nm. These peaks are characteristic of the near band edge and the deep-level emissions, respectively. Among all the samples, the one obtained at the time of 1 h roughly shows higher intensity in both of the PL peaks, and this sample was assigned for the study of antibacterial, antifungal, and anticancer activity.

Table 1 depicts the results obtained from the quantitative evaluation of the antibacterial and antifungal activity of the nanocomposite calcinated at 1 h against various organisms, including Escherichia coli (E. coli), Staphylococcus aureus, and Candida albicans. Their images are also demonstrated in Figure 8.

A colony-forming unit (CFU) is a parameter used to determine the number of organisms. Referring to Table 1, the number of Escherichia coli bacteria detected before the contact with blank and TiO_2-ZnO nanocomposite samples was 1.78×10^5 ml. However, after 24 hours of contact, the results changed remarkably. Accordingly, a CFU of 3.22×10^8 ml was acquired for the blank sample, much higher than the one obtained before the contact.

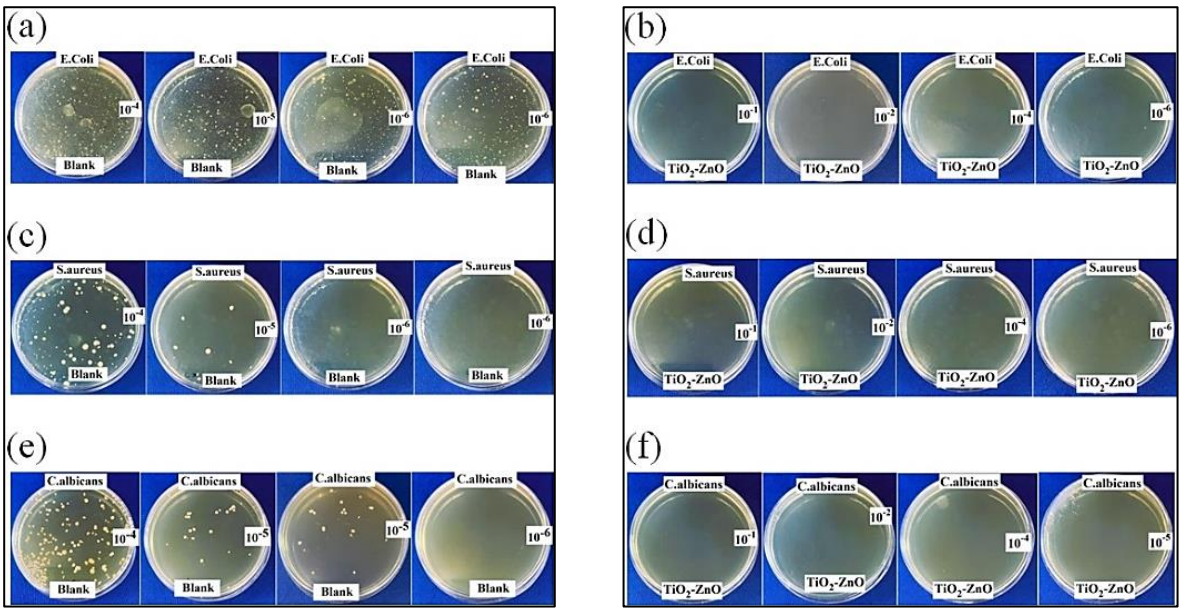

Fig. 8. The antibacterial and antifungal activity of the blank sample and the nanocomposite against different microorganisms

[DOI: 10.22068/ijmse.3778]

Table 1. Antibacterial and antifungal properties of the nanocomposite at the time of 1 h against different microorganisms

Microorganism	Sample	CFU (ml) at zero contact time	Sample Concentration (mg/ml)	Contact Time (h)	CFU/ml	Reduction (%)
Escherichia coli	TiO_2-ZnO	1.78×10^5	8	24	< 10	>99.99999%
	Blank		8		3.22×10^8	-
Staphylococcus Aureus	TiO_2-ZnO	3.1×10^5	8	24	< 10	>99.999%
	Blank		8		1.8×10^6	-
Candida albicans	TiO_2-ZnO	6.00×10^4	8	24	< 10	>99.999%
	Blank		8		3.25×10^6	-

On the other hand, the number of Escherichia coli bacteria considerably decreased after contact with TiO_2-ZnO nanocomposite for 24 h. In this regard, the CFU exhibited by the TiO_2-ZnO nanocomposite against Escherichia coli bacteria was less than 10 ml, equal to a reduction of >99.99999%. This means that our fabricated nanocomposites are immensely effective against E. coli. The absence of the nanocomposite had no impact on the reduction of the bacteria, and the blank sample had no antibacterial activity. The superb performance of TiO_2-ZnO nanocomposites in antibacterial tests can be related to their high capability in cell wall destruction, and metal-based nanoparticles typically demonstrate high activity against microorganisms [29].

In addition to Escherichia coli, Staphylococcus aureus bacteria were also chosen to examine the antibacterial activity of nanocomposites. Before exposure to samples, the CFUs recorded for both of the blank and TiO_2-ZnO nanocomposites were 3.1×10^5 ml. After 24 h contact with the blank sample, the number of Staphylococcus aureus bacteria increased and the CFU reached 1.8×10^6 ml, implying that the sample devoid of TiO_2-ZnO nanocomposite had no antibacterial activity. But, in the TiO_2-ZnO nanocomposite, a reduction of >99.999% occurred in the number of Staphylococcus aureus bacteria and the CFU for this sample decreased from 3.1×10^5 ml to less than 10 ml. Consequently, our proposed TiO_2-ZnO nanocomposites benefit from extraordinary antibacterial activity against different types of bacteria.

Candida albicans is a kind of fungus employed to study the antifungal properties of nanocomposites. As the data in Table 1 clearly shows, the number of Candida albicans fungi detected before the contact with the 8 mg/ml blank sample and the sample with TiO_2-ZnO nanocomposite was 6.00×10^4 ml. However, after 24-hour contact with the blank sample, the number of Candida albicans fungi increased remarkably, and it reached from 6.00×10^4 ml to 3.25×10^6 ml. The inclusion of TiO_2-ZnO nanocomposite into the sample led to a >99.999% reduction in the number of Candida albicans fungi. In this direction, the CFU reduced from 6.00×10^4 ml to less than 10 ml, attesting to the excellent antifungal properties of our prepared nanocomposites. As the results of the effectiveness of nanocomposites against microorganisms testified, our fabricated nanocomposites are hugely effective against bacteria and fungi. Moreover, the calcination time did not affect the activity of the nanocomposites.

In addition to the quantitative evaluation, the effectiveness of the nanocomposites calcinated at different times against various organisms, including E. coli, Staphylococcus aureus, and Candida albicans, was also examined using a disk diffusion test. The zone of inhibition of the samples against E. coli bacteria is brought in Table 2.

No antibacterial activity is observed for the distillated water (blank) sample. However, the samples containing TiO_2-ZnO nanocomposites showed high effectiveness against Escherichia coli bacteria. Raising the calcination time decreased the zone of inhibition, reducing the samples' effectiveness against bacteria. The best results were acquired for the nanocomposites calcinated at the time of 1 h. According to literature, increasing the calcination time can result in agglomeration of the particles, which can subsequently diminish the antibacterial activities of the samples [30]. As the FESEM images of our fabricated samples demonstrated, some agglomerated particles appeared for the nanocomposites calcinated at 2.5 and 3 hours, which negatively affected their antibacterial activities.

The antibacterial activity of our fabricated nanocomposites was compared with gentamicin. The activity of the sample prepared at 1 hour

[DOI: 10.22068/ijmse.3778]

is comparable with gentamicin. The zone of inhibition of the samples against Staphylococcus aureus bacteria is depicted in Table 3. Like the Escherichia coli bacteria, the blank sample exhibited no antibacterial activity against Staphylococcus aureus bacteria.

On the other hand, by inclusion of the TiO_2-ZnO nanocomposites into the diffusion disks, antibacterial activity is observed for the samples. All the TiO_2-ZnO nanocomposites calcinated at the times of 1, 1.5, 2, 2.5, and 3 h revealed antibacterial activity against Staphylococcus aureus bacteria, and the best results were obtained for the one fabricated at 1 h. Interestingly, an increment in the calcination time has resulted in a reduction in the antibacterial activity. The effectiveness of the nanocomposites synthesized at 1 h is comparable with the diffusion disk containing gentamicin. The zone of inhibition of the samples against Candida albicans fungi can be found in Table 4. Accordingly, the blank sample showed no effectiveness against Candida albicans fungi. However, the samples prepared at various calcination times revealed antifungal activity, and the one obtained at the time of 1 h showed the best antifungal activity. Increasing the calcination time has led to a reduction of antifungal activity. Besides, the effectiveness of the nanocomposites synthesized at the time of 1 h is comparable with the diffusion disk containing clotrimazole.

Table 2. Zone of inhibition of the samples against Escherichia coli bacteria

Sample	The diameters of the inhibition zones (mm)	Number of Tests	Concentration
1 h	19	1	100 µl
	19	2	
1.5 h	17	1	100 µl
	18	2	
2 h	18	1	100 µl
	16	2	
2.5 h	14	1	100 µl
	15	2	
3 h	13	1	100 µl
	15	2	
Gentamicin	28	1	30 µl
	27.5	2	
	28	3	
Distillated water	No	1	100 µl
	No	2	
	No	3	

Table 3. Inhibition zone of the samples against Staphylococcus aureus

Sample	The diameters of the inhibition zones (mm)	Number of Test	Concentration
1 h	21	1	100 µl
	20	2	
1.5 h	20	1	100 µl
	20	2	
2 h	19	1	100 µl
	18	2	
2.5 h	15	1	100 µl
	16	2	
3 h	13	1	100 µl
	15	2	
Gentamicin	31	1	30 µg
	31	2	
	31	3	
Distillated water	No	1	100 µl
	No	2	
	No	3	

[DOI: 10.22068/ijmse.3778]

Table 4. Inhibition zone of the samples against Candida albicans

Sample	The diameters of the inhibition zones (mm)	Number of Test	Concentration
1 h	15	1	100 µl
	16	2	
1.5 h	16	1	100 µl
	14	2	
2 h	15	1	100 µl
	13	2	
2.5 h	14	1	100 µl
	12	2	
3 h	12	1	100 µl
	10	2	
Gentamicin	20	1	50 µg
	19	2	
	20	3	
Distillated water	No	1	100 µl
	No	2	
	No	3	

The anticancer activity of the TiO_2-ZnO Nanocomposites calcinated at the time of 1 h was studied using an MTT assay, the results of which are shown in Table 5. In addition, the effects of various concentrations of TiO_2-ZnO nanocomposite on skin cell lines are demonstrated in Figure 9. The MTT assay was carried out after 24 h incubation. According to Table 5, the control sample (free of TiO_2-ZnO nanocomposite) shows a viability of 100%. On the other hand, the introduction of 15.625 µg/ml TiO_2-ZnO nanocomposite has decreased cell viability. Accordingly, the cell viability decreased from 100% to 99.55%, meaning that the TiO_2-ZnO nanocomposite can be effective against cancer cells. The increment in the dosage of TiO_2-ZnO nanocomposites increased their cytotoxicity activity or decreased the cell viability (Figure 10). In this regard, increasing the concentration of TiO_2-ZnO nanocomposite from 15.625 to 31.25 µg/ml decreased the cell viability from 99.55% to 97.24%. Besides, for the concentrations of 62.5, 125, and 250 µg/ml, cell viabilities of 90.45, 70.26, and 45% were respectively obtained, showing that increasing the amount of the TiO_2-ZnO nanocomposite can have a positive impact on their anticancer activity. The sample exhibited the best cytotoxicity activity with a 500 µg/ml concentration. Accordingly, including 500 µg/ml TiO_2-ZnO nanocomposite decreased the cell viability to 34.47%. As a consequence, our TiO_2-ZnO nanocomposites prepared at the time of 1 h can be a good inhibitor for the growth of cancer cells.

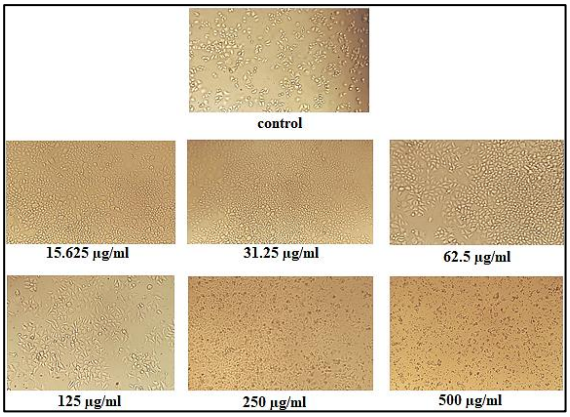

Fig. 9. The effect of TiO_2-ZnO nanocomposite calcinated at the time of 1 h on skin cell line after 24 h by inverted microscope

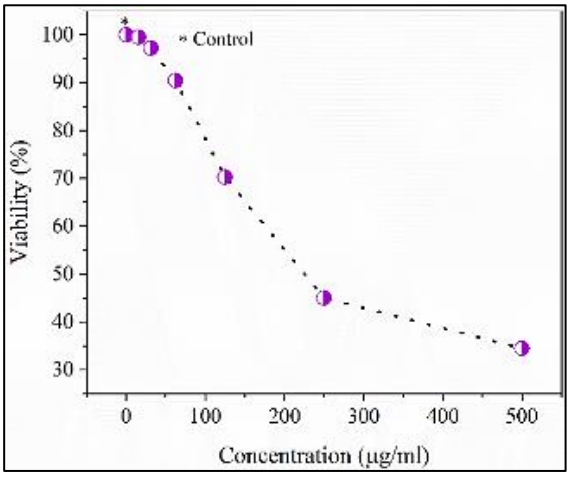

Fig. 10. The relative cell viability was recorded at various amounts of the nanocomposite calcinated at 1 hour.

[DOI: 10.22068/ijmse.3778]

Table 5. The anticancer activity of the nanocomposites prepared at 1 hour was examined by MTT assay

Concentration (µg/ml)	Control	15.625	31.25	62.5	125	250	500
Viability (%)	100	99.55	97.24	90.45	70.26	45	34.47

4. CONCLUSIONS

In our study, TiO_2-ZnO nanocomposites with different calcination times were successfully fabricated and characterized. Five calcination times, including 1, 1.5, 2, 2.5, and 3 h were adopted in this regard. Several characterization tests, consisting of XRD, FESEM, and EDXS, were employed to investigate the influence of calcination time on the nanocomposites' structure and morphology.

In accordance with the XRD images of all fabricated samples, the peaks related to anatase titanium dioxide and wurtzite zinc oxide were easily found. The aforementioned peaks corroborated the fabrication of the TiO_2-ZnO nanocomposites. Calcination time influenced inconsiderably the XRD patterns of the samples and subsequently their crystallite structures. Like the XRD analysis, the FESEM test confirmed the preparation of the TiO_2-ZnO nanocomposites where the round-shaped and rod-shaped structures were respectively attributed to the TiO_2 and ZnO nanoparticles. It was deemed that the increasing the calcination time up to 2.5 hours can result in production of more agglomerated nanoparticles. The results obtained from the EDXS technique were in consistent with the XRD and FESEM analyses where the peaks pertinent to the titanium and zinc elements were evidently detected. No change was seen in the EDXS patterns of all the TiO_2-ZnO nanocomposites. Raman spectroscopy also attested the existence of TiO_2 and ZnO where the vibrations of anatase titanium dioxide and also zinc oxide particles were detected. As the characterization tests of XRD, FESEM, EDXS and Raman spectroscopy verified, all the TiO_2-ZnO nanocomposites calcinated at the various times of 1, 1.5, 2, 2.5, and 3 h were synthesized and the calcination time can have insignificant impact on the morphology and structure of the nanocomposites.

In accordance with the UV-Visible spectra of all the TiO_2-ZnO nanocomposites taken to examine their optical property, a strong and broad absorption peak was vividly detected in the wavelength ranging from 300 to 400 nm. This peak was located in the UV region and exhibited the band gap absorption edge. Like the diffuse UV-Visible spectroscopy, all the nanocomposites manifested similar PL spectra. Accordingly, the peak at the wavelength of 700 nm in the UV region and the peak at the wavelength of 350 nm in the visible region were observed for all the nanocomposites. Also, based on PL spectroscopy, the nanocomposite prepared at the time of 1 h showed the best optical property, and was chosen for studying antibacterial and antifungal activity. In addition, the samples obtained at the time of 1 h decreased the number of different organisms, which verified their outstanding antibacterial and antifungal activity. This sample also revealed excellent cytotoxicity activity against the cancer cells. As a result, our proposed TiO_2-ZnO nanocomposites can be appropriate for optical applications and beneficial for their antibacterial, antifungal, and cytotoxicity activity. They can offer substantial potential for various applications such as medicine, environmental science, and more.

REFERENCES

[1]. Chaudhary, A., Kumar, N., Kumar, R., Salar, R.K., "Antimicrobial activity of zinc oxide nanoparticles synthesized from Aloe vera peel extract". SN Applied Sciences 2019, 1, 1-9.

[2]. Raj, L., Jayalakshmy, E., "A biogenic approach for the synthesis and characterization of zinc oxide nanoparticles produced by Tinospora cordifolia". Int J Pharm Pharm Sci 2015, 7, 384-386.

[3]. Gunasekaran, A., Rajamani, A.K., Masilamani, C., Chinnappan, I., Ramamoorthy, U., Kaviyarasu, K.J.C., "Synthesis and characterization of ZnO doped TiO_2 nanocomposites for their potential photocatalytic and antimicrobial applications". Catalysts 2023, 13, 215.

[4]. Ghamarpoor, R., Fallah, A., Jamshidi, M.J.A.o., "A review of synthesis methods, modifications, and mechanisms of ZnO/ TiO_2-based photocatalysts for

[DOI: 10.22068/ijmse.3778]

photodegradation of contaminants". ACS omega 2024, 9, 25457-25492.
[5]. Ilkhechi, N.N., Mozammel, M., Khosroushahi, A.Y.J.P.B., "Physiology, Antifungal effects of ZnO, TiO_2 and ZnO-TiO_2 nanostructures on Aspergillus flavus". Pestic. Biochem. Physiol. 2021, 176, 104869.
[6]. Mozammel, M., Khoroushahi, A.Y., "Antifungal effects of ZnO, TiO_2 and ZnO-TiO_2 nanocomposite on Aspergillus flavus". 2020.
[7]. Sarathi, R., Sheeba, N., Essaki, E.S., Sundar, S.M., "Titanium doped Zinc Oxide nanoparticles: A study of structural and optical properties for photocatalytic applications". Materials Today: Proceedings 2022, 64, 1859-1863.
[8]. Dathan, P.C., Nallaswamy, D., Rajeshkumar, S., Joseph, S., Ismail, S., Ajithan, L., Jose, L., "A Review on Biomedical Applications of Titanium Dioxide". Trends in Biomaterials & Artificial Organs 2023, 37, 49-54.
[9]. Pragathiswaran, C., Smitha, C., Barabadi, H., Al-Ansari, M.M., Al-Humaid, L.A., Saravanan, M., "TiO_2@ZnO nanocomposites decorated with gold nanoparticles: Synthesis, characterization and their antifungal, antibacterial, anti-inflammatory and anticancer activities". Inorganic Chemistry Communications 2020, 121 108210.
[10]. Chakra, C.S., Rajendar, V., Rao, K.V., Kumar, M., "Enhanced antimicrobial and anticancer properties of ZnO and TiO_2 nanocomposites". 3 Biotech 2017, 7 1-8.
[11]. Rajendran, R., Mani, A., "Photocatalytic, antibacterial and anticancer activity of silver-doped zinc oxide nanoparticles". Journal of Saudi Chemical Society 2020, 24 1010-1024.
[12]. Ahmed, N., Tanveer, K., Younas, Z., Yousaf, T., Ikram, M., Raja, N.I., Mashwani, Z.-u.-R., Alghamdi, S., Al-Moraya, I.S., Shesha, N.T., "Green-processed nano-biocomposite (ZnO–TiO_2): Potential candidates for biomedical applications". Green Processing and Synthesis 2023, 12, 20230076.
[13]. Nguyen, T.A., Nguyen, T.V., Nguyen-Tri, P., "Effect of Silver Decoration and Light Irradiation on the Antibacterial Activity of TiO_2 and ZnO Nanoparticles". 2019.
[14]. Akhavan, O., "Lasting antibacterial activities of Ag–TiO_2/Ag/a-TiO_2 nanocomposite thin film photocatalysts under solar light irradiation". Journal of colloid and interface science 2009, 336, 117-124.
[15]. Mohapatra, S., Nguyen, T.A., Nguyen-Tri, P., "Noble metal-metal oxide hybrid nanoparticles: Fundamentals and applications". Elsevier, 2018.
[16]. Daou, I., Moukrad, N., Zegaoui, O., Rhazi Filali, F.J.W.S., "Antimicrobial activity of ZnO-TiO_2 nanomaterials synthesized from three different precursors of ZnO: influence of ZnO/TiO_2 weight ratio". Water Sci Technol 2018, 77, 1238–1249.
[17]. Siwińska-Stefańska, K., Kubiak, A., Piasecki, A., Dobrowolska, A., Czaczyk, K., Motylenko, M., Rafaja, D., Ehrlich, H., Jesionowski, T.J.A.S.S., "Hydrothermal synthesis of multifunctional TiO_2-ZnO oxide systems with desired antibacterial and photocatalytic properties". Appl. Surf. Sci. 2019, 463, 791-801.
[18]. Johra, F.T., Jung, W.-G.J.A.C.A.G., "RGO–TiO_2–ZnO composites: synthesis, characterization, and application to photocatalysis". Applied Catalysis A: General 2015, 491, 52-57.
[19]. Prasannalakshmi, P., Shanmugam, N.J.M.S.i.S.P., "Fabrication of TiO_2/ZnO nanocomposites for solar energy driven photocatalysis". Mater. Sci. Semicond. Process. 2017, 61, 114-124.
[20]. Sethi, D., Sakthivel, R., "ZnO/TiO_2 composites for photocatalytic inactivation of Escherichia coli". Journal of Photochemistry & Photobiology, B: Biology 2017, 168, 117-123.
[21]. Wang, N., Li, X., Wang, Y., Hou, Y., Zou, X., Chen, G.J.M.L., "Synthesis of ZnO/TiO_2 nanotube composite film by a two-step route". Materials Letters 2008, 62, 3691-3693.
[22]. Das, D., Mondal, P.J.R.a., "Low temperature grown ZnO: Ga films with predominant c-axis orientation in wurtzite structure demonstrating high conductance, transmittance and photoluminescence". RSC advances 2016, 6, 6144-6153.
[23]. Rafiq, M.Y., Iqbal, F., Aslam, F., Bilal, M.,

[DOI: 10.22068/ijmse.3778]

Munir, N., Sultana, I., Ashraf, F., Manzoor, F., Hassan, N., Razaq, A., "Fabrication and characterization of ZnO/MnO_2 and ZnO/TiO_2 flexible nanocomposites for energy storage applications". J. Alloys Compd. 2017, 729, 1072-1078.

[24]. Jun, M.-C., Park, S.-U., Koh, J.-H.J.N.r.l., "Comparative studies of Al-doped ZnO and Ga-doped ZnO transparent conducting oxide thin films". Nanoscale research letters 2012, 7, 1-6.

[25]. Mousa, H.M., Alenezi, J.F., Mohamed, I.M., Yasin, A.S., Hashem, A.F.M., Abdal-Hay, A., Synthesis of TiO_2@ZnO heterojunction for dye photodegradation and wastewater treatment". J. Alloys Compd. 2021, 886, 161169.

[26]. Kurudirek, S.V., Kurudirek, M., Klein, B.D.B., Summers, C.J., Hertel, N.E., "Methods in Physics Research Section A: Accelerators, Detectors, A. Equipment, Synthesis and photoluminescence properties of Ga-doped ZnO nanorods by a low temperature solution method". Nucl. Instrum. Methods Phys. Res. A 2018, 904, 158-162.

[27]. Al-Asedy, H.J., Bidin, N., Abbas, K.N., Al-Azawi, M.A., "Structure, morphology and photoluminescence attributes of Al/Ga co-doped ZnO nanofilms: Role of annealing time". Mater. Res. Bull 2018, 97, 71-80.

[28]. Phan, D.T., Farag, A.A.M., Yakuphanoglu, F., Chung, G.S., "Optical and photo-luminescence properties of Ga doped ZnO nanostructures by sol-gel method". J. Electroceramics 2012, 29, 12-22.

[29]. Pragathiswaran, C., Smitha, C., Abbubakkar, B.M., Govindhan, P., Krishnan, N.A., "Synthesis and characterization of TiO_2/ ZnO–Ag nanocomposite for photocatalytic degradation of dyes and anti-microbial activity". Materials Today: Proceedings 2021, 45, 3357-3364.

[30]. Ismail, A.M., Menazea, A.A., Kabary, H.A., El-Sherbiny, A.E., Samy, A., "The influence of calcination temperature on structural and antimicrobial characteristics of zinc oxide nanoparticles synthesized by Sol–Gel method". Journal of Molecular Structure 2019, 1196, 332-337.

[DOI: 10.22068/ijmse.3778]